during only the first weeks following an AIDS virus infection may provide sufficient protection against central memory CD4+ T cell loss to confer a survival advantage to infected individuals. Moreover, current models of large human HIV-1 vaccine efficacy trials propose the use of set-point viral load and total CD4+ T lymphocyte count as surrogate markers for a beneficial vaccine effect (22, 23). It has been presumed that a lower set-point viral load or a higher set-point CD4+ T lymphocyte count after infection will portend a better AIDS-free survival. The results of the present study indicate that set-point viral load and total CD4+ T lymphocyte count may not have predictive value in this setting. Rather, the quantitation of central memory CD4+ T cells in a vaccine trial several months after infection may be an important immune correlate of long-term protection and predict the efficacy of an HIV-1 vaccine.

Most important, this cohort of vaccinated monkeys followed for 850 days after challenge with the highly pathogenic SIVmac251 provides a distinctive data set for exploring the mechanisms underlying the vaccine-associated survival. The demonstration of an association between the magnitude of the vaccine-elicited immune responses and the duration of survival after challenge provides a framework for understanding the immune protection conferred by cellular immune–based vaccines. Moreover, the prolonged survival conferred by a vaccine that stimulates T cell immunity provides support for pursuing clinical efficacy trials of such HIV-1 vaccines, even if they do not induce sterilizing immunity.

References and Notes

1. N. L. Letvin, *Annu. Rev. Med.* **56**, 213 (2005).
2. J. W. Mellors *et al.*, *Science* **272**, 1167 (1996).
3. D. H. Barouch *et al.*, *Science* **290**, 486 (2000).
4. R. R. Amara *et al.*, *Science* **292**, 69 (2001).
5. J. W. Shiver *et al.*, *Nature* **415**, 331 (2002).
6. Y. Nishimura *et al.*, *Proc. Natl. Acad. Sci. U.S.A.* **101**, 12324 (2004).
7. I. Ourmanov *et al.*, *J. Virol.* **74**, 2740 (2000).
8. P. Polacino *et al.*, *J. Virol.* **73**, 618 (1999).
9. P. S. Polacino *et al.*, *J. Virol.* **73**, 8201 (1999).
10. J. D. Lifson *et al.*, *J. Virol.* **71**, 9508 (1997).
11. D. R. Casimiro *et al.*, *J. Virol.* **79**, 15547 (2005).
12. T. U. Vogel *et al.*, *J. Virol.* **77**, 13348 (2003).
13. N. L. Letvin *et al.*, *J. Virol.* **78**, 7490 (2004).
14. S. Santra *et al.*, *J. Virol.* **79**, 6516 (2005).
15. M. S. Seaman *et al.*, *J. Virol.* **79**, 2956 (2005).
16. Materials and methods are available as supporting material on *Science* Online.
17. R. Pal *et al.*, *J. Virol.* **76**, 292 (2002).
18. M. S. Seaman *et al.*, *J. Virol.* **79**, 4580 (2005).
19. Y. Sun *et al.*, *J. Immunol.* **174**, 4753 (2005).
20. J. J. Mattapallil *et al.*, *Nature* **434**, 1093 (2005).
21. R. S. Veazey *et al.*, *J. Virol.* **74**, 57 (2000).
22. P. B. Gilbert *et al.*, *J. Infect. Dis.* **192**, 974 (2005).
23. T. Hulgan *et al.*, *J. Infect. Dis.* **192**, 950 (2005).
24. This work was supported in part with funds from the intramural research program of the Vaccine Research Center, NIAID, NIH.

Long-Term Potentiation of Neuron-Glia Synapses Mediated by Ca2+-Permeable AMPA Receptors

Woo-Ping Ge,[1,2]* Xiu-Juan Yang,[1,2]* Zhijun Zhang,[1,2] Hui-Kun Wang,[1,2] Wanhua Shen,[1,2] Qiu-Dong Deng,[1,2] Shumin Duan[1]†

Interactions between neurons and glial cells in the brain may serve important functions in the development, maintenance, and plasticity of neural circuits. Fast neuron-glia synaptic transmission has been found between hippocampal neurons and NG2 cells, a distinct population of macroglia-like cells widely distributed in the brain. We report that these neuron-glia synapses undergo activity-dependent modifications analogous to long-term potentiation (LTP) at excitatory synapses, a hallmark of neuronal plasticity. However, unlike the induction of LTP at many neuron-neuron synapses, both induction and expression of LTP at neuron-NG2 synapses involve Ca2+-permeable AMPA receptors on NG2 cells.

Glial cells in the central nervous system (CNS) constitute a heterogeneous population of cell types. Macroglia-like NG2 cells express the chondriotin sulfate proteoglycan NG2 and have been described as oligodendrocyte precursor cells (OPCs) or given other names (1–3). NG2 cells in the CA1 area of the hippocampus receive direct glutamatergic and γ-aminobutyric acid (GABA)–ergic synaptic inputs from neurons (4, 5). The structure of the neuron-glia synapses found in NG2 cells differs from that of neuronal synapses by having a less well-defined postsynaptic density and smaller presynaptic boutons that contain fewer vesicles (4). With the exception of developing neuromuscular junctions (6), long-term potentiation (LTP) has been observed only at synapses between neurons. Thus it is of interest to examine whether the neuron-NG2 cell synapses have adequate expression and localization of components required for both the induction and expression of LTP.

Whole-cell recordings were made from NG2 cells in the CA1 region of rat hippocampal slices. Glial cell membrane currents induced by the stimulation of Schaffer collaterals (SCs) were used to monitor rapid neuron-glial signaling. The identity of astrocytes and NG2 cells was determined by both electrophysiological recording and immunostaining. Staining with antibodies to glial fibrillary acidic protein (GFAP) and NG2 revealed two distinct non-overlapping cell populations (fig. S1) (4). NG2 cells were identified by having a relatively high input resistance (131.7 ± 5.4 megohms, $n = 160$ cells), large transient A-type currents (I_A) and delayed rectifier K+ currents (I_K), and small tetrodotoxin (TTX)–sensitive Na+ currents that failed to generate typical action potentials (Fig. 1 and fig. S1D) (4, 7). We found no detectable voltage-dependent Ca2+ currents in these cells (Fig. 1, F and G). When cells with the above characteristics were marked by intracellular loading with biocytin or lucifer yellow and subsequently immunostained with an antibody against NG2, all of the cells (14 out of 14) were found to be NG2-positive (fig. S1).

Electrical stimulation of SCs, in the presence of the GABA type A (GABA_A) receptor antagonist bicuculline, elicited inward currents in NG2 cells with rapid kinetics (Fig. 2A; rise time, 0.71 ± 0.06 ms; decay time, 2.13 ± 0.17 ms; $n = 11$), which was consistent with the existence of direct monosynaptic inputs made by SCs on NG2 cells (4). The excitatory postsynaptic currents (EPSCs) exhibited short-term plasticity similar to that induced at SC-CA1 pyramidal cell synapses, as suggested by the paired pulse ratio (PPR) of these two types of synapses over a broad range of paired pulse intervals (Fig. 2B). The EPSCs were reversibly abolished by the application of kynurenic acid (Kyn) (Fig. 2D and fig. S1E), a broad-spectrum blocker of ionotropic glutamate receptors. These EPSCs were due to the activation of non-*N*-methyl-D-aspartate receptors (NMDARs), because the antagonist 6,7-dinitroquinoxaline-2,3-dione (DNQX) completely abolished the responses, whereas the NMDARs antagonist

[1]Institute of Neuroscience and Key Laboratory of Neurobiology, Shanghai Institutes for Biological Sciences, Chinese Academy of Sciences, Shanghai 200031, China. [2]Graduate School of the Chinese Academy of Sciences, Shanghai 200031, China.

*These authors contributed equally to this work.
†To whom correspondence should be addressed. E-mail: shumin@ion.ac.cn

D,L-2-amino-5-phosphonovaleric acid (APV) had no effect on these currents recorded at +40 mV to remove the Mg^{2+} block of NMDAR (Fig. 2, C and D).

Most AMPARs in the CNS are Ca^{2+}-impermeable because of the presence of the GluR2 subunit, although GluR2-lacking AMPARs have been observed in some developing and mature neurons as well as in glial cells (*4*, *8*, *9*). Consistent with the previous finding that NG2 cells contain Ca^{2+}-permeable AMPA receptors (CaPARs) (*4*), we found that EPSCs observed in NG2 cells were significantly reduced by philanthotoxin-433 (PhTx), a toxin that specifically blocks the CaPARs (*10*) (Fig. 2D). Currents mediated by CaPARs display inward rectification, exhibiting a reduction of outward currents at depolarizing membrane potentials because of a voltage-dependent block by intracellular polyamines (*8*, *9*). To estimate the proportion of the EPSC component mediated by CaPARs, we examined the rectification of EPSCs by monitoring the ratio of EPSCs recorded at –60 mV to that at +40 mV (I_{-60}/I_{+40}). The rectification of EPSCs was stronger in 1-week-old rats [(postnatal day 8 (P8) to P10] than that in rats at P13 to P15 and P19 to P21. Furthermore, the proportion of EPSCs inhibited by 30 to 50 µM 1-naphthylacetyl spermine (NAS), a synthetic analog of Joro spider toxin that selectively blocks CaPARs (*11*), was also larger in young animals, suggesting a developmental reduction in the EPSC mediated by CaPARs (Fig. 2, E and F). To directly estimate the glutamate-induced Ca^{2+} influx through CaPARs, NG2 cells were loaded with the Ca^{2+} dye Rhod-2, and the hippocampal slices were perfused with glutamate in the presence of cyclothiazide, which blocks the desensitization of AMPARs. We found that glutamate-induced currents and Ca^{2+} elevations were largely abolished by DNQX and significantly reduced by NAS. Thus, a large proportion of glutamate-induced Ca^{2+} elevation in NG2 cells is mediated by CaPARs (Fig. 2, G to I). The residual Ca^{2+} elevation in the presence of NAS may be caused indirectly by the activation of (i) Ca^{2+}-impermeable AMPARs that may induce Ca^{2+} elevation through a Na^+-Ca^{2+} exchanger and (ii) metabotropic glutamate receptors that mobilize intracellular Ca^{2+} stores. Because the perfusion of glutamate activates both synaptic and extrasynaptic AMPARs, the finding that NAS caused stronger inhibition of glutamate-induced current (Fig. 2I) than of SC-induced EPSCs (Fig. 2F) suggests that CaPARs are more prevalent in extrasynaptic AMPARs. In some experiments, Ca^{2+} elevation in NG2 cells induced by the stimulation of SCs was also detected by line scanning with a high temporal resolution (fig. S2).

Evoked EPSCs in NG2 cells were compared before and after tetanic or theta burst stimulation (TBS) of the SCs. Although tetanic stimulation failed to induce an apparent change in EPSCs (Fig. 3H and fig. S3C), TBS resulted in a persistent increase in the EPSC amplitude in NG2 cells (Fig. 3, A and B), analogous to LTP found at neuronal synapses. The effectiveness of TBS in LTP induction at NG2 synapses may be attributed to the fact that these EPSCs exhibited substantial amplitude reduction during tetanic stimulation but not during TBS (fig. S3), which may result in a higher amount of Ca^{2+} influx during TBS than during tetanic stimulation. Bath application of APV, which largely abolishes CA1 neuronal LTP (*12–14*), did not affect TBS-induced "glial LTP" (gLTP) of SC-NG2 cell synapses (Fig. 3, C, G, and H). In contrast, application of TBS during a brief period of perfusion with Kyn resulted in no change in EPSCs in NG2 cells (Fig. 3, E, G, and H), suggesting that TBS-induced gLTP requires the activation of nonNMDA receptors.

Intracellular Ca^{2+} elevation is critical for LTP induction at many synapses (*13*). We
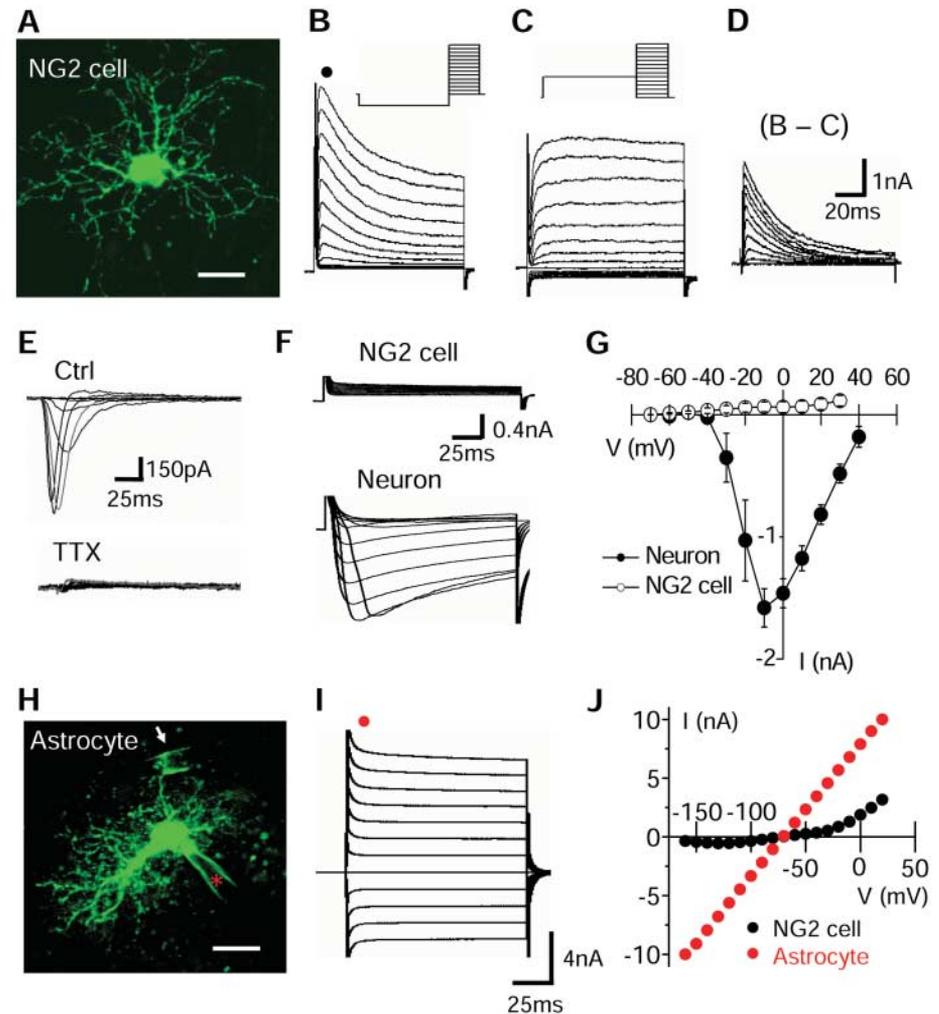
Fig. 1. Electrophysiological properties of NG2 cells. (**A**) Three-dimensional reconstruction of a typical NG2 cell identified electrophysiologically. The cell was loaded with Oregon-green 488 BAPTA-1 in the CA1 region of a living hippocampal slice. Scale bar, 10 µm. (**B**) and (**C**) Outward currents recorded from an NG2 cell evoked by step voltages (100 ms, 10 mV) from −80 to +50 mV with a prepulse of −120 mV (B) or −30 mV (C) for 300 ms. In (B), the black circle indicates the position of peak currents as measured in (J). (**D**) Isolated I_A reached by subtracting (C) from (B). (**E**) Transient inward currents recorded from an NG2 cell induced by the same voltage pulses as in (B) in the presence of K^+ channel blockers with or without TTX. (**F**) and (**G**) Voltage-dependent Ca^{2+} currents were recorded in neurons but not in NG2 cells. In (G), error bars for neurons (solid circles, $n = 8$ cells) and for NG2 cells (open circles, $n = 7$ cells) indicate SEM. (**H**) Morphology of a typical astrocyte identified electrophysiologically. The cell was loaded and imaged as in (A). White arrow indicates the end-feet of the astrocyte enwrapping a microvessel. Red asterisk indicates the dye-containing pipette. Scale bar, 10 µm. (**I**) Current responses from an astrocyte evoked by step voltages (100 ms, 20 mV) from −160 to +20 mV. Red circle indicates the position of peak currents as measured in (J). (**J**) Example current-voltage relation curves constructed from recordings as shown in (B) (peak current) and (I).
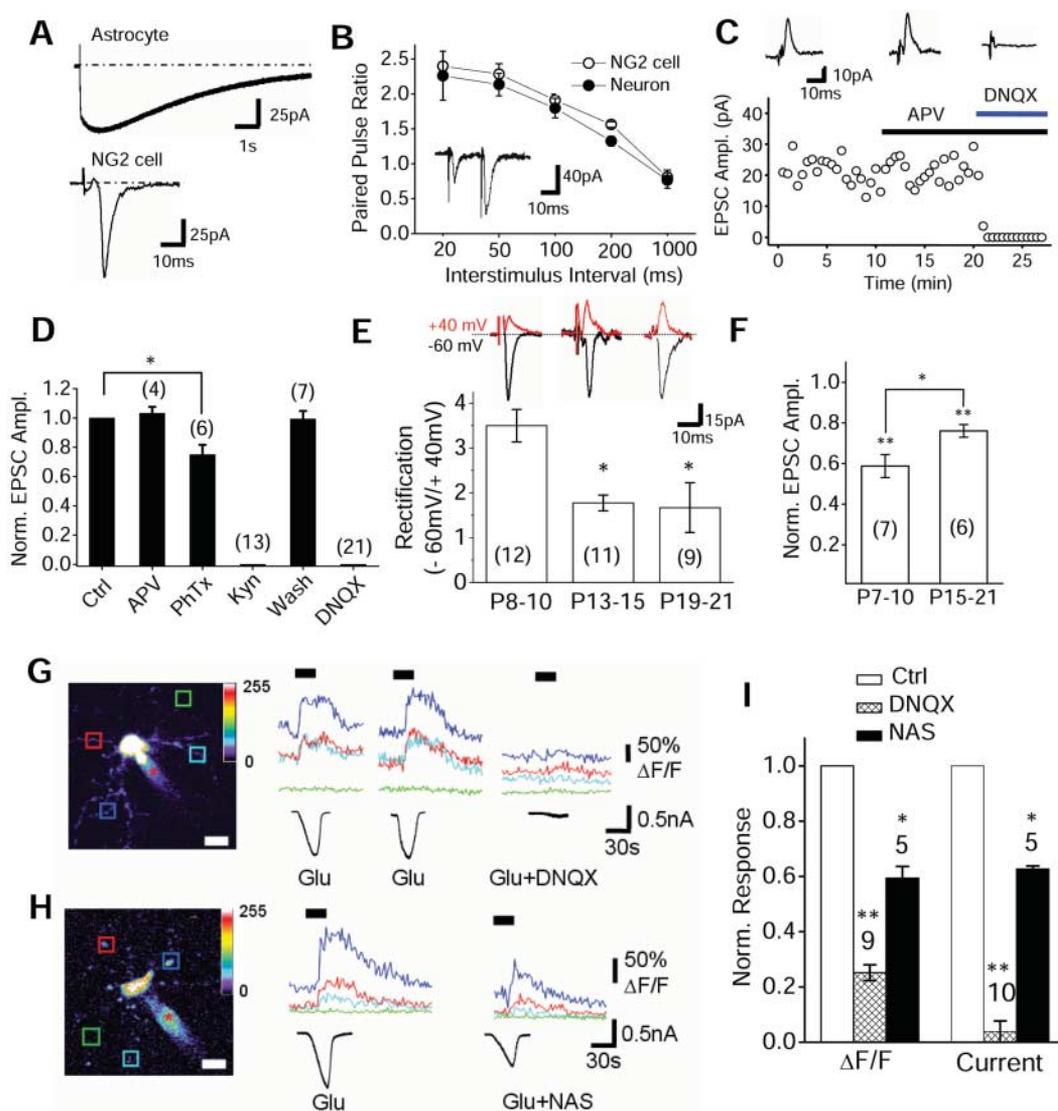
found that TBS failed to induce gLTP when NG2 cells were loaded with a fast Ca^{2+} chelator [1,2-bis(2-aminophenoxy)ethane-N,N,N',N'-tetraacetic acid (BAPTA)]. A persistent reduction in the EPSC amplitude was observed instead (Fig. 3, D, G, and H). This reduction may result from an incomplete Ca^{2+} buffering in the fine processes of NG2 cells where SC-NG2 synapses are located, suggesting potential bidirectional Ca^{2+}-dependent plasticity (13) at these synapses. Given the lack of voltage-gated Ca^{2+} current in these NG2 cells (Fig. 1, F and G), we further examined whether CaPARs are responsible for the Ca^{2+} influx required for gLTP induction. Application of PhTx completely prevented the induction of gLTP by TBS (Fig. 3, F to H). This gLTP is

likely to be expressed as an increased glutamate response in NG2 cells, because PPRs were not significantly changed after gLTP induction (Fig. 4, A and B), suggesting no presynaptic change in glutamate release probability (13).

The trafficking of GluR1-containing AMPARs plays a crucial role in the expression of NMDAR-dependent LTP (15, 16). Induction of NMDAR-dependent LTP in CA1 neurons, which do not express CaPARs, did not change the rectification of AMPAR-mediated EPSCs unless neurons were overexpressed with green fluorescent protein-GluR1 (16); this finding suggests that, after LTP induction, the endogenous GluR1 subunits are trafficked to synapses in heteromeric forms containing GluR2, so that the increased AMPARs are also Ca^{2+}-

impermeable. Activation of CaPARs by tetanic stimulation at cerebellar stellate cell synapses results in a prolonged decrease in the rectification of AMPAR-mediated EPSCs due to the replacement of CaPARs with Ca^{2+}-impermeable receptors (17, 18), leading to a decreased Ca^{2+} influx and EPSC amplitude recorded at the physiological membrane potential (–60 mV), a plasticity that may resemble the long-term depression and represent a protective mechanism. Synaptic strengthening induced by the activation of the CaPARs has been reported in some dorsal horn neurons (19) and amygdala interneurons (20), but it is not clear whether the proportion of the CaPAR-mediated EPSCs is changed after LTP induction in these synapses. We found that TBS

Fig. 2. Properties of EPSCs and glutamate-induced responses in NG2 cells. (**A**) Example traces showing SC stimulation-induced fast response in an NG2 cell (bottom) and slow response in an astrocyte (top). (**B**) PPRs in NG2 cells and CA1 pyramidal neurons induced by SC stimulations at various interstimulus intervals ($n = 7$ pairs). Insets represent example recordings from an NG2 cell. (**C**) Inhibition of EPSCs in an NG2 cell by DNQX (10 μM) but not by APV (100 μM). Insets from left to right represent sample traces (average of five traces) from control, perfusion with APV, and APV plus DNQX, respectively. (**D**) Summary data from experiments as shown in (C). Each column represents averaged data of EPSCs recorded during 5-min perfusion (or washout) of antagonists. Data are normalized with the control (averaged EPSC amplitude during initial 5-min recording before drug application). *, $P < 0.05$. (**E**) Averaged rectification of SC-NG2 EPSCs from hippocampal slices at different development stages. Insets show example EPSCs recorded at +40 mV (red) and –60 mV (black). * ($P < 0.01$) indicates significance as compared with P8–10 group. (**F**) Averaged EPSCs in the presence of NAS. Data are normalized with control EPSCs (before NAS application). Significance as compared with the control group (**$P < 0.001$) or between the two groups (*$P < 0.05$) is indicated. (**G**) and (**H**) Imaging of glutamate-induced Ca^{2+} elevation in NG2 cells. Left panels depict NG2 cells filled with Rhod-2 through a patch pipette (red asterisks). Right panels provide example traces for glutamate-induced Ca^{2+} signal (color traces) and current recording (black traces) in the absence or presence of DNQX (G) and NAS (H). Traces in different colors in the right panel correspond to the imaged regions in the left panel marked by squares of the same color. Black bars indicate perfusion of 500 μM glutamate (Glu). (**I**) Summarized data of glutamate-induced current and Ca^{2+} fluorescent change ($\Delta F/F$; see supporting online material) and current as shown in (G) and (H). * ($P < 0.01$) and ** ($P < 0.001$) indicate significance as compared with the control group.

induced an increased rectification of EPSCs (Fig. 4C), suggesting an increased function or proportion of CaPARs at these synapses. Loading NG2 cells with spermine caused more rectification of SC-induced EPSCs (Fig. 4, compare C with D), suggesting that endogenous polyamines are sufficient (21) but not saturating in inducing inward rectification of AMPAR currents. Furthermore, the induction of gLTP in NG2 cells loaded with spermine also resulted in an increased rectification of EPSCs (Fig. 4D). Such synaptic modification will increase not only the amplitude of synaptic responses but also Ca^{2+} influx and subsequent activation of Ca^{2+}-dependent intracellular signaling. The

intracellular C terminal of the proteoglycan NG2 has been reported to bind with the PDZ domain of GRIP1 (22), an adaptor protein important for AMPAR trafficking and synaptic plasticity (18). It is possible that the interaction of NG2 proteoglycan and GRIP1 in these glial cells played a role in the trafficking of CaPARs found in the present study.

The conversion of CaPARs into Ca^{2+}-impermeable receptors at Bergmann glial cells, by transfection with the GluR2 subunit, results in the retraction of glial processes that ensheath synapses and multiple innervations of Purkinje cells by climbing fibers (23). Pathological insults such as ischemia also down-regulate

GluR2 expression in OPCs and neurons (24), leading to the expression of CaPARs and enhanced glutamate toxicity after ischemia. Thus, an adequate level of activity by CaPARs is important for maintaining normal synaptic structure and function. Glutamate receptor activation is linked to the proliferation and differentiation of OPCs (25), and NG2 cells can differentiate into neurons both in vitro and in vivo (26, 27). The expression of gLTP and the elevation of CaPARs in SC-NG2 synapses may thus contribute to activity-dependent neuronal regulation of NG2 cell differentiation. Like astrocytes (12, 28, 29), NG2 cells may also secrete neuroactive factors to regulate neuronal
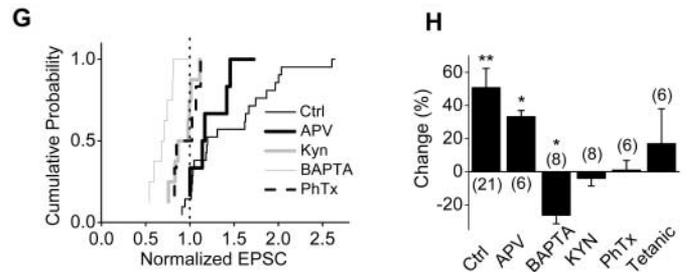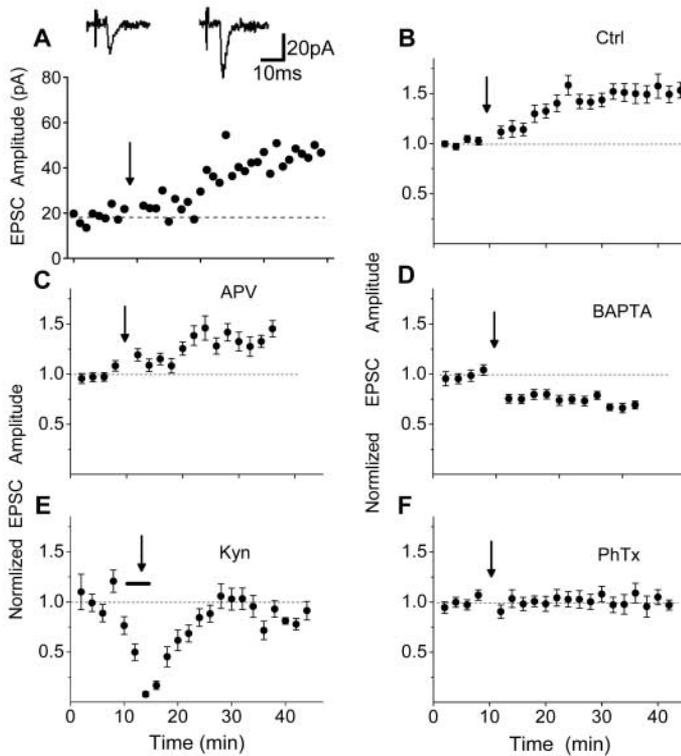
Fig. 3. Persistent enhancement of EPSCs in NG2 cells induced by TBS of SCs. Example (**A**) and summarized (**B**) data showing the TBS (arrows)–induced gLTP at NG2 cell synapses are shown. Insets in (A) are sample traces before and after TBS, respectively. (**C** to **F**) Summary data showing the time course of EPSCs before and after TBS in the presence of 100 μM APV (C), 0.5 mM Kyn (E) applied during the period indicated by the bar, 4 μM PhTx (F), or 10 mM intracellular BAPTA in NG2 cells (D). (**G**) Cumulative distribution of EPSC amplitudes after TBS as shown in (B) to (F). Data are normalized with the average EPSC amplitude (vertical dotted line) before TBS for each recording. (**H**) Summary of results showing averaged percent changes in EPSC amplitudes estimated during the period from 15 to 20 min after TBS or tetanic stimulation. * ($P < 0.05$) and ** ($P < 0.01$) indicate significant changes in EPSC amplitude after induction.
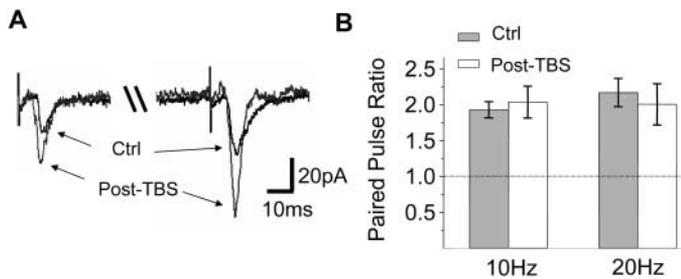
Fig. 4. Comparing EPSC properties in an NG2 cell before and after TBS. (**A**) Example EPSC recordings from an NG2 cell showing similar PPR (10 Hz) recorded before and after TBS application. (**B**) Summary of averaged PPR at 10 Hz ($n = 5$ cells) and 20 Hz ($n = 4$ cells) before and after TBS induction. (**C** and **D**) Summary of the rectification of EPSCs examined before and after TBS induction in NG2 cells loaded with [(D) $n = 7$] or without [(C) $n = 7$] 0.1 mM spermine. Insets, example EPSCs from an NG2 cell recorded at +40 and −60 mV, respectively, before and after TBS induction. * ($P < 0.05$) and ** ($P < 0.01$) indicate significance between the control and post-TBS groups.
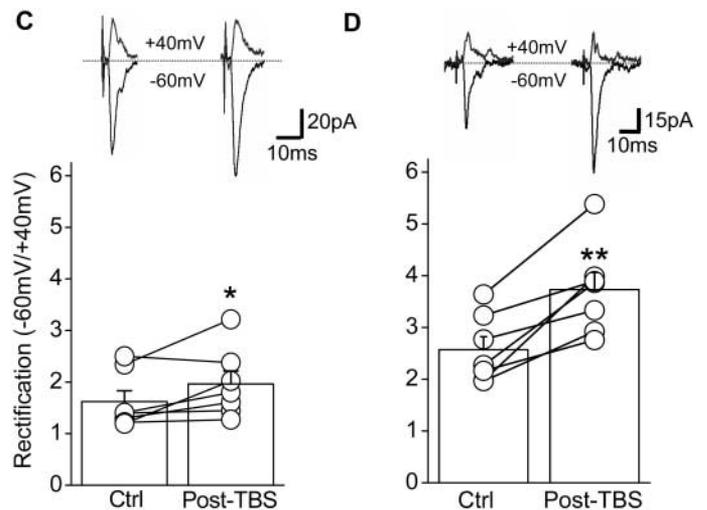
functions. Rapid neuron-NG2 cell signaling may allow rapid feedback regulation of neuronal functions by Ca^{2+}-dependent secretion of neuroactive factors, and the strength of such feedback regulation will increase after the induction of gLTP.

References and Notes

1. J. M. Levine, J. P. Card, *J. Neurosci.* **7**, 2711 (1987).
2. J. M. Levine, R. Reynolds, J. W. Fawcett, *Trends Neurosci.* **24**, 39 (2001).
3. M. C. Raff, R. H. Miller, M. Noble, *Nature* **303**, 390 (1983).
4. D. E. Bergles, J. D. Roberts, P. Somogyi, C. E. Jahr, *Nature* **405**, 187 (2000).
5. S. C. Lin, D. E. Bergles, *Nat. Neurosci.* **7**, 24 (2004).
6. J. Wan, M. Poo, *Science* **285**, 1725 (1999).
7. R. Chittajallu, A. Aguirre, V. Gallo, *J. Physiol.* **561**, 109 (2004).
8. S. K. Kamboj, G. T. Swanson, S. G. Cull-Candy, *J. Physiol.* **486**, 297 (1995).
9. D. S. Koh, J. R. Geiger, P. Jonas, B. Sakmann, *J. Physiol.* **485**, 383 (1995).
10. M. S. Washburn, R. Dingledine, *J. Pharmacol. Exp. Ther.* **278**, 669 (1996).
11. M. Koike, M. Iino, S. Ozawa, *Neurosci. Res.* **29**, 27 (1997).
12. Y. Yang *et al.*, *Proc. Natl. Acad. Sci. U.S.A.* **100**, 15194 (2003).
13. T. V. Bliss, G. L. Collingridge, *Nature* **361**, 31 (1993).
14. J. S. Diamond, D. E. Bergles, C. E. Jahr, *Neuron* **21**, 425 (1998).
15. R. Malinow, R. C. Malenka, *Annu. Rev. Neurosci.* **25**, 103 (2002).
16. Y. Hayashi *et al.*, *Science* **287**, 2262 (2000).
17. S. Q. Liu, S. G. Cull-Candy, *Nature* **405**, 454 (2000).
18. S. J. Liu, S. G. Cull-Candy, *Nat. Neurosci.* **8**, 768 (2005).
19. J. G. Gu, C. Albuquerque, C. J. Lee, A. B. MacDermott, *Nature* **381**, 793 (1996).
20. N. K. Mahanty, P. Sah, *Nature* **394**, 683 (1998).
21. S. H. Shi *et al.*, *Science* **284**, 1811 (1999).
22. J. Stegmuller, H. Werner, K. A. Nave, J. Trotter, *J. Biol. Chem.* **278**, 3590 (2003).
23. M. Iino *et al.*, *Science* **292**, 926 (2001).
24. D. E. Pellegrini-Giampietro, J. A. Gorter, M. V. Bennett, R. S. Zukin, *Trends Neurosci.* **20**, 464 (1997).
25. V. Gallo *et al.*, *J. Neurosci.* **16**, 2659 (1996).
26. M. C. Nunes *et al.*, *Nat. Med.* **9**, 439 (2003).
27. A. Aguirre, V. Gallo, *J. Neurosci.* **24**, 10530 (2004).
28. J. M. Zhang *et al.*, *Neuron* **40**, 971 (2003).
29. A. Araque, G. Carmignoto, P. G. Haydon, *Annu. Rev. Physiol.* **63**, 795 (2001).
30. We thank M. Poo for critical comments on the manuscript and W. Zhou, Q. Hu, D. Xiang, J. Zhao, and J. Mao for technical assistance. This work was supported by the National Natural Science Foundation of China (grant 30321002) and Major State Basic Research Program of China (grant G200077800).

Language Control in the Bilingual Brain

J. Crinion,[1] R. Turner,[1] A. Grogan,[1] T. Hanakawa,[2,3] U. Noppeney,[4] J. T. Devlin,[5] T. Aso,[3] S. Urayama,[3] H. Fukuyama,[3] K. Stockton,[1] K. Usui,[3] D. W. Green,[6] C. J. Price[1]*

How does the bilingual brain distinguish and control which language is in use? Previous functional imaging experiments have not been able to answer this question because proficient bilinguals activate the same brain regions irrespective of the language being tested. Here, we reveal that neuronal responses within the left caudate are sensitive to changes in the language or the meaning of words. By demonstrating this effect in populations of German-English and Japanese-English bilinguals, we suggest that the left caudate plays a universal role in monitoring and controlling the language in use.

People who communicate in more than one language can voluntarily control which language is in use at any given time. The bilingual brain can, for example, determine the language of heard or written speech, produce words in the selected language, and inhibit the production of words in the non-selected language. All of these processes necessitate language-sensitive neuronal activity. Contrary to expectation, however, whole-brain functional neuroimaging studies have shown that highly proficient bilinguals activate the same set of brain regions irrespective of which language is presented or produced; see (*1*) a for recent review. These findings suggest that the neural circuits for different languages are highly overlapping and interconnected but do not indicate how the brain determines or controls the language in use.

Our study was designed to identify language-dependent neuronal responses at the level of word meanings (i.e., semantics). By using whole-brain functional neuroimaging, semantic priming, and the neuronal adaptation technique (*2–4*), we expected to see regional reductions in left anterior temporal activation when two successively presented written words had similar meanings (e.g., trout-SALMON) compared with different meanings (e.g., trout-HORSE) (*5*, *6*). Critically, if semantic activation is independent of the language of the stimuli, then neuronal adaptation will be the same irrespective of whether the semantically related words are in the same or different languages (*2*). If, on the other hand, a region responds to both semantic content and the language of the stimuli, then neuronal adaptation will depend on whether semantically related words are presented in the same or different languages.

Our participants saw visually presented sequential word pairs (e.g., trout-SALMON). They were instructed to ignore the first (the prime) and to make a decision based on the meaning of the second [the target, printed in capitals (English and German) or a larger font (Japanese) (Materials and Methods)]. A short interval (250 ms) between the onsets of the prime and the target was chosen to minimize the likelihood that the prime could be used to predict the target word but to maximize the time available to activate semantic associations in both languages (*7*). The influence of the prime on the target was identified by comparing the response to prime-target pairs that were either semantically related (bathtub-SHOWER) or unrelated (spoon-SHOWER). We then identified language-dependent semantic responses by comparing the effect of semantic priming when prime and target were in the same language (trout-SALMON in English or forelle-LACHS in German) or different languages (e.g., trout-LACHS or forelle-SALMON). Lastly, to identify the semantic system that was common to all types of priming, we included a baseline condition with meaningless non-linguistic symbols. Our two-by-two-by-two experimental design manipulated (i) the language of the target word and varied whether the prime and the target were (ii) semantically related or unrelated and (iii) written in the same or different languages.

The robustness and universality of the observed effects were ensured by including three groups of highly proficient bilinguals (table S1). One group of German-English bilinguals ($n = 11$) participated in a positron emission tomography (PET) experiment, whereas a second group of German-English bilinguals ($n = 14$) and a third group of Japanese-English bilinguals ($n = 10$) participated in functional magnetic resonance imaging (fMRI) experiments. The stimuli in all three experiments were carefully equated across languages (table S2). Therefore, language-dependent neuronal responses present in all three groups would provide strong evidence for the universality of the language mechanism, particularly because

[1]Wellcome Department of Imaging Neuroscience, University College London, London WC1N 3BG, UK. [2]Department of Cortical Function Disorders, National Center of Neurology and Psychiatry, Tokyo 187-8502, Japan. [3]Human Brain Research Center, Kyoto University, Kyoto 606-8507, Japan. [4]Max Planck Institute for Biological Cybernetics, 72076 Tübingen, Germany. [5]Centre for Functional Magnetic Resonance Imaging of the Brain, University of Oxford, Oxford OX3 9DU, UK. [6]Department of Psychology, University College London, London WC1E 6BT, UK.

*To whom correspondence should be addressed. E-mail: c.price@fil.ion.ucl.ac.uk